Remote Sensing of Environment 205 (2018) 46–55

Contents lists available at ScienceDirect

Remote Sensing of Environment

journal homepage: www.elsevier.com/locate/rse

Climate and nutrient effects on Arctic wetland plant phenology observed from phenocams

Andresen C.G.[a,b,*], Tweedie C.E.[a], Lougheed V.L.[a]

[a] Department of Biological Sciences, The University of Texas at El Paso, El Paso, TX 79968, USA
[b] Los Alamos National Laboratory, Los Alamos, NM 87545, USA

ARTICLE INFO

Keywords:
Phenocams
Arctic wetlands
Ponds
Aquatic plants
Nutrients
Greenness
Biomass
NDVI
Time lapse
Climate variability
Carex aquatilis
Arctophila fulva

ABSTRACT

This study explores how climate and nutrients influence productivity of arctic wetland plants. The Green-excess Index (GEI) derived from Red, Green and Blue digital image brightness values from digital repeat photography (a.k.a. phenocams) was used to track the inter-annual variability in seasonal greening and above ground biomass for two dominant aquatic emergent graminoids on the Arctic Coastal Plain of northern Alaska: *Carex aquatilis* and *Arctophila fulva*. Four years of seasonal and inter-annual greening trends show strong differences in timing and intensity of greenness among species. Thawing degree-days (TDD, days above 0 °C) was a good predictor of GEI in both *A. fulva* and *C. aquatilis*. Employing regression tree analyses, we found a greening threshold of 46 TDD for *A. fulva*, after which GEI increased markedly, while *C. aquatilis* greened more gradually with a greening mid-point of 31 TDD. Based on long-term climate records and TDD thresholds, greening date has begun 16 thawing degree-days earlier over the past 70 years. To understand the effects of latitude and nutrients on seasonal greening, we compared southern sites and nutrient enriched sites with reference sites. We found statistically higher greenness in southern sites and enriched sites compare to reference sites in both plant species, supporting the role of nutrients and warmer temperatures as key factors enhancing productivity in arctic wetlands. In addition, this study provides an inexpensive, alternative method to monitor climate and nutrient effects at high frequency in arctic aquatic systems through camera-derived GEI greenness and has the potential to bridge the gap between plot level and satellite based observations given its strong relationships with biomass and NDVI.

1. Introduction

Wetlands represent a significant portion of the Arctic landscape (Lehner and Döll, 2004; Woo and Young, 2006; Avis et al., 2011; Melton et al., 2013). These systems are characterized by supporting aquatic vegetation through saturated hydrological conditions and ponding of water sustained by the shallow permafrost layer (Cowardin et al., 1979). These systems are oasis for productivity in this polar desert environment where timing, extent, and magnitude of plant primary productivity play a fundamental role in arctic hydrology, carbon fluxes and energy balance (Prowse et al., 2006; Westergaard-Nielsen et al., 2013; Andresen and Lougheed, 2015). For example, the increase in wetland plant biomass and cover in tundra ponds over recent decades (Andresen and Lougheed, 2015), has been associated with increased nutrient availability (Lougheed et al., 2011; Reyes and Lougheed, 2015) and longer thaw season, resulting in a significant rise of methane emissions to the atmosphere (Andresen et al., 2017). With the continuing and projected warming of the Arctic over the next century, there is uncertainty with respect to how changes in plant biomass and phenology in Arctic wetlands will contribute to or mitigate warming. Given the increasingly realized importance of arctic change on global processes (Hinzman et al., 2013), documenting these responses to shifts in climate is essential for assessing potential climatic feedbacks at regional and global scales.

Plot-scale phenological measurements can provide detailed observations on seasonal trends and changes at the species-level (Elmendorf et al., 2012; Oberbauer et al., 2013). However, plot-level measurements are often labor-intensive and logistically difficult in the Arctic. Spectral vegetation indices from satellite-based remote sensing, such as the Normalized Difference Vegetation Index (NDVI), have shown to be a reliable method for estimating regional and continental scale changes in Arctic greening (Bhatt et al., 2010; Epstein et al., 2012; Walker et al., 2012). However, the limited temporal coverage and persistent cloud cover in the Arctic restricts detailed seasonal satellite observations (Stow et al., 2004). Furthermore, the majority of publicly available imagery also lacks the geospatial accuracy and resolution

* Corresponding author at: MS J495, Los Alamos, NM 87545, USA.
E-mail address: candresen@lanl.gov (C.G. Andresen).

https://doi.org/10.1016/j.rse.2017.11.013
Received 15 May 2017; Received in revised form 6 November 2017; Accepted 10 November 2017

required for time series analysis of discreet plant communities (Andresen et al., 2017). Defining novel technologies to advance understanding of fine-scale phenological dynamics in the highly heterogeneous and remote region of the Arctic tundra landscape is needed to address these challenges. Technological advances in sensor systems and instrument platforms to monitor phenological dynamics such as handheld spectrometers and thermal cameras, have been become increasingly popular recent years (Healey et al., 2014). However, these systems are often costly and highly technical, limiting their use in ecological studies. Therefore, there is a need to develop cost- and time-efficient mid-scale methods suitable for tracking seasonal and inter-annual plant biomass trends and bridging the gap between plot and satellite-level observations (Nijland et al., 2016).

Repeat photography has become a well-sourced tool for documenting long-term changes in Arctic vegetation (Sturm et al., 2001; Tape et al., 2006; Callaghan et al., 2011; Villarreal et al., 2012), including aquatic systems (Smol and Douglas, 2007; Andresen and Lougheed, 2015; Andresen et al., 2017). However, these camera systems have not yet been used to assess seasonal dynamics. Mostly outside the Arctic, analysis of digital time-lapse photography (phenocam imagery) has developed as a favored method for near-surface remote sensing and generally provides high spatial and temporal resolution for the characterization of plant phenophase development and greenness as proxies of plant biomass (Richardson et al., 2009; Brown et al., 2016). Previous studies have employed commercial phenocams to assess seasonal and inter-annual greening trends in a wide range of ecosystems including desert scrublands (Kurc and Benton, 2010), subalpine grassland (Migliavacca et al., 2011), low Arctic fen (Westergaard-Nielsen et al., 2013) and forests (Richardson et al., 2009; Elmore et al., 2012; Keenan et al., 2014; Nagai et al., 2016). Greenness indices derived from Red-Green-Blue (RGB) color space such as the green excess index (GEI) and the green chromatic coordinate (G%) have proven to be good indicators of gross primary production (GPP) and leaf area index (LAI) (Ahrends et al., 2009; Richardson et al., 2009; Saitoh et al., 2012; Keenan et al., 2014). To our knowledge, no studies have directly linked RGB indices to aboveground biomass nor tested its potential in vegetated aquatic systems. Additionally, this technology appears to not have been used for assessing plant phenological responses to different environmental conditions, such as gradients of temperature and nutrients, which are key determinants of ecosystem carbon balance in arctic tundra plant communities (Walker et al., 2006; Epstein et al., 2012). Nutrients in particular, have been increasing over the past four decades in tundra ponds (Lougheed et al., 2011) boosting plant growth and methane emissions (Andresen and Lougheed, 2015; Andresen et al., 2017). However, little is known about how nutrients affect seasonal changes in timing and intensity of greening and senescing in Arctic tundra wetlands. Therefore, it is imperative to understand and characterize nutrient effects in aquatic plant phenology and develop novel methods to identify and monitor these effects.

In this multi-year study, focused on wetlands in the northern Arctic Coastal Plain of Alaska, we evaluate the effectiveness of time-lapse digital photography as a novel automated and cost-effective method to assess:

(i) Seasonal and inter-annual greening patterns of aquatic emergent graminoids,
(ii) The effects of latitude and nutrient gradients on the timing and magnitude of wetland plant greenness, and
(iii) The relationship between phenocam-derived greenness, biomass and NDVI derived from a hyperspectral spectrometer.

2. Methods

2.1. Research site

This study was located on the Arctic Coastal Plain area near Utqiaġvik (formerly known as Barrow) and Atqasuk, Alaska. The region is characterized by its low-relief, deep permafrost, shallow thaw depth, and the dominance of thaw lakes and basins that contain numerous wetlands and ponds (Hinkel et al., 2003; Lougheed et al., 2011; Andresen and Lougheed, 2015). This Arctic landscape (~71° latitude) is known for its short snow-free growing season lasting approximately three months from early June to the beginning of September with an average summer temperature of 4 °C. The annual vegetation growing cycle starts with warmer temperatures and 24 h of light in late May-early June triggering snow melt, and thawing of the active layer, suitable conditions for plant growth. Peak growing season is usually reached in late July–early August followed by senescence and decreasing temperature and daylight hours (Gamon et al., 2013). In late September, snow starts covering the vegetated areas and ice develops gradually freezing shallow ponds and wetlands systems throughout the water column.

Aquatic vegetation communities in the Arctic Coastal Plain are dominated by two emergent graminoids: *Arctophila fulva* and *Carex aquatilis*. *A. fulva* has a wide distribution across Arctic and Boreal regions, and is common in inundated landscapes where competition from other species is lacking (Dobson, 1989). *Carex aquatilis* is known for its wide distribution across northern hemisphere wetland habitats. These perennial species usually grow in pure stands with depth preference of 16.2 cm for *A. fulva* and 4.5 cm for *C. aquatilis* and (Andresen and Lougheed, 2015) and are the most important primary producers in Utqiaġvik tundra ponds (McRoy and Leue, 1973). Both species have been noted to be increasing in both areal cover and tiller density in the Utqiaġvik area (Andresen et al., 2017).

For the purpose of this study, we monitored nine tundra pond sites (Table 1), including five sites that were representative reference sites for Utqiaġvik, AK (IBP-J, IBP-C, IBP-10, ITEX-N, WL03), one nutrient enriched thermokarst pond (TK3), one nutrient enriched urban pond (BOXER) and two ponds located approximately 100 km south of Utqiaġvik near the village of Atqasuk, AK (ATQ-E, ATQ-W). Given that Utqiaġvik air temperature is expected to continue its upward trajectory over the next century and air temperature in Atqasuk is ~4 °C warmer than Utqiaġvik (http://climate.gi.alaska.edu/), we used sites in Atqasuk as a proxy for the future state of Utqiaġvik ponds. All ponds in this study contained *A. fulva* and *C. aquatilis*, except for ponds IBP-C and TK3, which contained only *C. aquatilis*. Three representative sites (IBP-C, J, 10) were monitored for three or four consecutive years, while the remaining sites were only monitored in 2013.

2.2. Nutrient enriched sites

Enriched urban ponds (e.g. Boxer) are located within the town of Barrow, AK and their source of nutrients is mainly from urban runoff. Enriched thermokarst ponds (e.g. TK3) were situated within the Barrow Environmental Observatory (BEO), and their nutrient inputs originate

Table 1
Location and classification of sites sampled in this study. Plant types include *Arctophila fulva* (A) and *Carex aquatilis* (C).

Site	Type	Latitude	Longitude	Plant type	Years
IBP-10	Reference	71.293500	−156.704330	A, C	2011–2013
IBP-J*	Reference	71.293630	−156.701440	A, C	2010–2013
IBP-C*	Reference	71.294600	−156.702100	C	2010–2013
ITEX-N	Reference	71.318140	−156.583220	A, C	2013
WL03	Reference	71.282300	−156.616250	A, C	2013
TK3	Enriched Thermokarst	71.273980	−156.636431	C	2013
BOXER	Enriched Urban	71.303620	−156.752594	A, C	2013
ATQ-E	Lower Latitude	70.447892	−157.362756	A, C	2013
ATQ-W	Lower Latitude	70.457525	−157.401083	A, C	2013

*Sites with Wingscapes BirdCam; all others sites used TimeLapseCam.

from permafrost slumping into ponds. We used soil P levels to verify enriched sites versus reference sites since P is the limiting nutrient for *A. fulva* and *C. aquatilis* (Andresen, 2014). For each pond, we combined three top soil samples (0–5 cm; ~1 kg total) from each vegetation cover type (e.g. *A. fulva* and *C. aquatilis*). We sampled additional enriched ponds for statistical purposes. Enriched sites (n = 4) contained significantly higher soil P (available P, Olsen NaHCO3 method) in areas covered by *A. fulva* (7.45 ± 3.13 mg/kg, $p < 0.001$) and *C. aquatilis* (5.15 ± 1.59 mg/kg, $p < 0.02$) compared to references sites (n = 8) with 3.47 ± 0.69 mg/kg for *A. fulva* and 3.13 ± 0.85 mg/kg for *C. aquatilis*. P concentrations in enriched site Boxer was 10.5 mg/kg and 4.4 mg/kg for *A. fulva* and *C. aquatilis*, respectively. P levels were 7.3 mg/kg for enriched site TK3 *C. aquatilis* (TK3 does not contain *A. fulva*).

2.3. Phenocams

We employed commercial time-lapse digital cameras as a near-surface remote sensing method to continuously acquire photographs and test their applicability for monitoring plant phenology and biomass of *A. fulva* and *C. aquatilis*. The cameras used in this project were either Wingscapes® WSCA02 BirdCam 2.0 or Wingscapes® TimeLapseCam 8.0 cameras, both with 8 megapixels size, 3264 pixels wide by 2448 pixels tall. Most sites were monitored using the TimeLapseCam except IBP-J and IBP-C, which used the BirdCam. Both cameras output 24-bit JPG files within Red-Green-Blue (RGB) color space. Each image is imbedded with site, date and time information. These cameras were selected because of their: (i) time-interval configuration, (ii) freeze proof and water resistant design and (iii) relatively low cost (approximately US $100–$150).

Cameras were mounted on heavy-duty tripods 2.5 m above ground level facing North and at a downward angle of approximately − 30 degrees from the horizon (Fig. 1). The cameras were programmed to trigger at 30 min intervals during the snow-free growing season from early June to late August–September. Daylight for this period is 24 h until August 2nd when the sun starts setting. In some cases, technical difficulties with battery life or camera error limited some seasonal observations and resulted in missing data (< 5% of total records). Seasonal end dates of image acquisition varied depending on the year and site access by local volunteers. Cameras with automatic exposure adjust to different light conditions; therefore, the output pixels represent relative brightness for each channel as opposed to total radiance values. To minimize influences of automatic camera settings in scene illumination, white balance was set constant and not automatic which greatly improves the consistency in RGB brightness values under variable light conditions (Richardson et al., 2009).

In order to assess the differences of GEI measured in an oblique angle (e.g. Phenocams) versus nadir angle, we acquired Kite Aerial Photography (Andresen et al., 2014) of IBP-J (Fig. 1) and IBP-C over the season and compared the Phenocam footprint GEI values (oblique angle) and the KAP GEI (nadir angle, matching the phenocam footprint area) for both plant species in IBP-J and only *C. aquatilis* in IBP-C.

2.4. Image processing

Images were analyzed for seasonal changes in the relative brightness of the Red, Green and Blue channels. User-defined regions of interest (ROIs) in the scene were selected to understand changes in channel brightness for areas dominated by different taxa (i.e. *A. fulva* or *C. aquatilis*). We averaged all pixels within an ROI for each channel and calculated the green excess index (GEI) (Richardson et al., 2009). Like other spectral indices (i.e. NDVI), GEI is a proxy for changes in greenness from growing biomass and leaf area in the region of interest (ROI) and reflects greening trends of the selected image area and not individual leaves in the image. The GEI index was calculated using the formula: $[2 * G - (R + B)]$ where G is the brightness value in the green channel, R is the brightness value in the red, and B is the brightness value in the blue. Daily averages were computed using only photos acquired within 6 h of solar noon (~14:00 h ADT) in order to capture the highest incident solar radiation. Daily averages were also used to minimize diurnal changes in light and weather conditions on vegetation. We excluded images affected by water condensation on the lens, which represented < 5% of all images.

To enable inter-comparison of RGB values among cameras, we assessed differences in RGB channel brightness by repeatedly photographing a gray calibration card commonly used for film, video and printer calibration (Digital Kolor Kard ®). All cameras were triggered simultaneously under identical sunny conditions. We determined the average offset factor in each channel from an assumed half-tone gray brightness value of 127 in an 8-bit RGB scale of 0–255. Cameras gray calibration card brightness resulted on an average (± SD) of 108 ± 10, 126.6 ± 10.4 and 127.8 ± 13.6 for Red, Green and Blue channels respectively. Both camera types showed similar channel brightness variability. After image processing, calculated RGB values were then corrected using the offset factor obtained for each camera.

2.5. Ancillary observations

In order to determine the utility of the cameras relative to more standard methods, we measured NDVI and above-ground plant biomass within the phenocam sampling footprints. Using the non-destructive allometric methods described in Andresen et al. (2017), we determined seasonal plant biomass of *A. fulva* (IBP-J, IBP-10) and *C. aquatilis* (IBP-C, IBP-J) within the phenocam footprint every 10 days over the growing

Fig. 1. (Left) Near-surface, oblique camera mounted on a tripod facing north at IBP Pond J, (middle) a sample photo taken from this system and (right) a kite aerial photograph of the site where camera location is marked with an X.

season (June–August) for 2010–2013. Field reflectance was collected from early June to late August of years 2011–2012 at IBP sites (IBP-10, IBP-C, IBP-J) employing a single channel portable spectrometer (JAZ, Ocean Optics). We minimize noise from non-linearity of photo response of the spectrometer pixels by using adequate integration times without saturating the measurements. In addition, we visually inspected each collection (including calibration) through a live feed into a portable computer with OceanView Software V1.4.5. Target radiance was cross-calibrated at every pond site using a certified 99% reflective white spectralon calibration standard (WS-1, Labsphere), which allowed for the estimation of the reflectance ratio between plot radiance and the calibration standard radiance. White calibration standard (38 mm wide) was set at a distance of 30 mm from the fiber (field of view of 25°) at each calibration, then capped closed to minimize degradation. Reflectance ratio measurements were acquired for each biomass plot (described above) with a circular footprint of ~1 m diameter at a nadir angle from terrain. We averaged NDVI measurements from 5 scans in each plot, and 4–6 plots per pond for every sampled date for comparison with the camera footprint GEI. Normalized Difference Vegetation Index (NDVI) was estimated from reflectance ratio values in the red and infrared wavelengths using the formula: NDVI = (800 nm − 680 nm) / (800 nm + 680 nm). NDVI has become a standard proxy of plant productivity and biomass in the Arctic and has been used to track plot (Boelman et al., 2005; Soudani et al., 2012; Gamon et al., 2013) to regional and global seasonal and decade time-scale greening trends (Jia, 2003; Bhatt et al., 2010; Walker et al., 2012; Zeng and Jia, 2013). To increase the robustness of the relationship between NDVI and biomass, we also included measurements collected in nearby ponds without phenocams (Lougheed et al., 2015).

To examine the relationships between NDVI, biomass and GEI, as well as the association of greening trends (e.g. GEI) and meteorological data, we used simple linear regressions as well as a partition analysis (i.e. regression tree analysis) to identify non-linear interactions (Keenan et al., 2014). Greening and senescence dates, defined as the dates where thresholds in greenness were observed, were determined using a regression tree analysis performed in JMP v11. In order to distinguish greening and senescence dates using a regression tree, we split the data into early summer (JD < 220) and late summer datasets (JD > 210 to 240) (Lougheed et al., 2007). Uncertainty in change points was expressed as a cumulative probability distribution determined by 1000 bootstrap estimates in R v3.3 (Lougheed et al., 2007). We also compared greening dates to meteorological data, including air temperature, precipitation, thawing degree-days (TDD; number of days above 0 °C), photosynthetic active radiation (PAR), wind speed and direction. The limited number of years (n = 4) sampled in this study prevented statistical predictions between mean annual phenological variables (e.g. greening date, peak season GEI) and environmental variables. Climate data over the study period was measured using a HOBO® weather station situated near site IBP-C from mid-June to mid-August. Long-term air temperature records are from the from Barrow airport (http://climate.gi.alaska.edu/).

3. Results

3.1. Greening date, peak greenness and senescence

Phenocams portrayed distinct seasonal greening date, peak greenness and senescence for *A. fulva* and *C. aquatilis*, as illustrated for reference sites in 2013 (Fig. 2). *Carex aquatilis* tended to green sooner than *A. fulva*, while both tend to senesce shortly after the sun began to set again on August 2nd. These differences were maintained between years, where analysis of GEI greening thresholds for reference sites sampled over several years (n = 3; IBP-C, -J, -10), showed that, on average, *C. aquatilis* had reached a greening threshold in late June (average JD = 182), 18 days before *A. fulva* (JD = 200) (Table 2). While *C. aquatilis* greened steadily until early July, greening of *A. fulva* was more abrupt and occurred in mid-July (average JD = 199) after a short reddening phase that dips *A. fulva* GEI values between days 190 and 200. Both *A. fulva* and *C. aquatilis* reached peak greenness in mid to late July, between days 200 and 210. Peak-season GEI values were different among plant species reaching values of 10–20 for *A. fulva* and 30–50 for *C. aquatilis*. Senescence of both species started in the second week of August (average JD = 223). *Carex aquatilis* senesced gradually to near zero GEI values as winter approached, while *A. fulva* senesced more rapidly, reaching minimum GEI due to strong plant reddening on days 250–260 (early September). Inter-annual comparison of greening thresholds for *A. fulva* and *C. aquatilis* found no years where the earliest or latest greening dates aligned for both species (Table 2), suggesting controls of greening differ among species.

GEI and NDVI were closely correlated for both *A. fulva* (R^2 = 0.58, $p < 0.01$) and *C. aquatilis* (R^2 = 0.88, $p < 0.001$)(Fig. 3). GEI was more strongly related to aboveground biomass than ground-based NDVI for both *A. fulva* (r^2 = 0.75, $p < 0.001$) and *C. aquatilis* (r^2 = 0.92, $p < 0.001$). NDVI was nonetheless also strongly correlated with biomass for *A. fulva* (r^2 = 0.61 $p < 0.01$) and *C. aquatilis* (r^2 = 0.79, $p < 0.001$). For both GEI and NDVI, the non-linear relationship with biomass suggests both indices progressively saturate above a biomass of 200 g/m^2.

Comparison between oblique phenocam GEI and nadir KAP GEI shows underestimation from nadir KAP angle (Fig. 4). However, peak season (1st week of Aug) GEI values for *C. aquatilis* show a closer 1:1 ratio at the upper end of the curve between which coincides with the highest biomass on the ground, and thus leaf area exposed to the sensor. *A. fulva* biomass and cover also increases during peak season but it is still sparse in the nadir view.

3.2. Environmental controls of greening

For sites sampled over multiple years, GEI during the greening period (JD < 220) was moderately associated with average daily water temperature for both *C. aquatilis* (r^2 = 0.25 $p < 0.0001$) and *A. fulva* (r^2 = 0.18 $p < 0.0001$). However, thawing degree-days (TDD, days above 0 °C) was a better predictor of GEI in both *A. fulva* (r^2 = 0.34 $p < 0.0001$) and *C. aquatilis* (r^2 = 0.69 $p < 0.0001$; Fig. 5). For *A. fulva*, in particular, there was a threshold thawing degree-day (46) after which GEI increased markedly; regression tree analysis of this threshold explained 16% more of the variation in GEI data (r^2 = 0.50; Fig. 5). We could also identify a threshold value at which *C. aquatilis* GEI increased (31); however, this regression tree explained slightly less variation than the linear model (r^2 = 0.60) shown in Fig. 5. For *A. fulva*, we found positive relationships of peak growing season biomass with greening date meaning that the earlier the greening date, less peak season biomass for that year (*A. fulva* Peak Biomass = 1.1477 * Greening date − 218.53, R^2 = 0.3189, $p < 0.01$. In *C. aquatilis* however, relationship were not significant.

In 2013, seasonal trends in GEI among reference sites (IBP-J, IBP-C, IBP-10, ITEX-N, WL3) were compared to cameras situated in enriched systems (BOXER,TK3) and Southern sites (ATQ-E, ATQ-W) (Fig. 6). On average, southern sites had the highest *C. aquatilis* GEI, which was most notable in early summer, followed by enriched sites, then reference sites (paired *t*-tests; $p < 0.0001$). Reference sites consistently maintained a lower average GEI in the mid- to late-summer. For *A. fulva*, southern and enriched site GEIs were not different from each other but were both significantly higher than reference sites (paired *t*-tests; $p < 0.0001$).

While there were differences in maximum GEI and biomass among site types, we observed little to no difference in greening dates. On average, *C. aquatilis* greening occurred two days earlier (day 185) in southern sites compared to the sites located near Utqiaġvik (reference and enriched; day 187); however, we could not compare these greening dates statistically. *A. fulva* showed no difference in greening date among site types (day 200). Similarly, there was only a 1 TDD difference

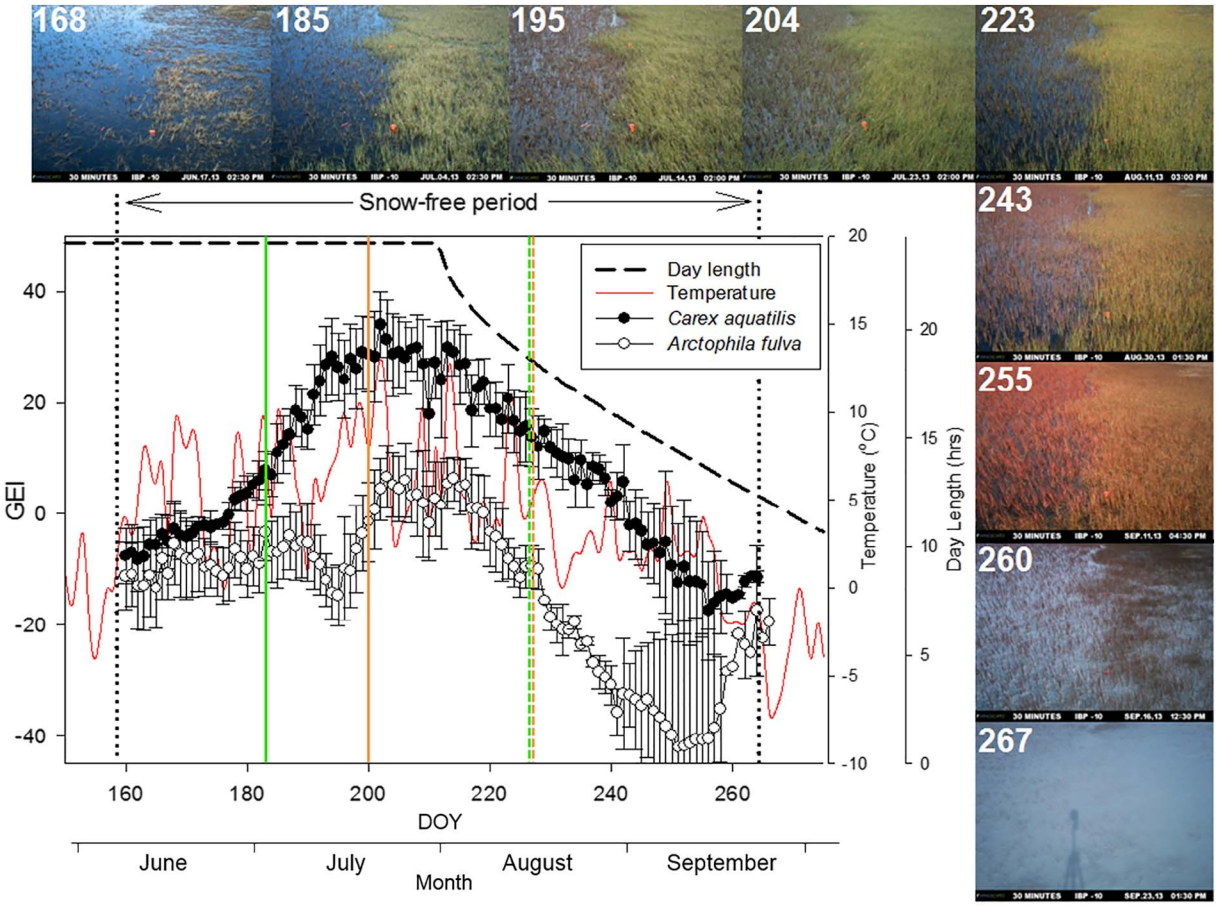

Fig. 2. Average seasonal GEI trends for *C. aquatilis* and *A. fulva* for reference sites in 2013 (n = 5). Vertical colored lines represent greening (solid line) and senescence dates (dashed line) for *C. aquatilis* (green) and *A. fulva* (orange). Seasonal photographs are for site IBP Pond 10, with *A. fulva* dominating the left half of the image and *C. aquatilis* the right half of the image. Numbers in the top left of each image depict the Julian day of image acquisition. (For interpretation of the references to color in this figure legend, the reader is referred to the web version of this article.)

Table 2
Average greening and senescing dates reported in Julian Days (JD ± SD), for reference, multi-year sites over the study period (2010 – 2013).

	Greening date		Senescing date	
Year	*C. aquatilis*	*A. fulva*	*C. aquatilis*	*A. fulva*
2010	183	205	221	223
2011	176	201	228	227
2012	185	193	224	222
2013	183	200	227	227
Averages	182 ± 4	200 ± 5	225 ± 3	225 ± 3

among greening dates among sites, with *C. aquatilis* greening on TDD = 35 in Utqiaġvik, and TDD = 36 in Atqasuk. For *A. fulva*, greening occurred on TDD = 49–50 in Utqiaġvik, and TDD = 51 in Atqasuk. These greening dates are comparable to those reported above for multi-year sites. The necessity of removing the southern cameras in early August limited the late-summer observations for Southern sites (ATQ-E, ATQ-W).

3.3. Retrospective analysis of greening date

We employed the TDD threshold for species greening dates described in Section 3.2 to model long-term (1945–2016) greening dates for each species based on climate records. The long-term trends in Fig. 7 show that greening date is approximately 16 days earlier over the 72 year period. Linear regression of the modeled greening dates indicates a decrease of more than − 0.2 days/year for greening date (*C. aquatilis* greening date = $-0.23 * \text{year} + 654$, *A. fulva* greening date = $-0.27 * \text{year} + 749$). We also found that thawing degree-days were strongly related to thaw depth (Not shown; Thaw depth = $3.1 + 0.55 * \text{TD}$, $R2 = 0.95$ $p < 0.0001$, $n = 28$).

4. Discussion

Four years of summer phenology monitoring using time-lapse photography effectively identified variability in greening trends among plant species, where the number of days above 0 °C played an important role in timing of greening, while nutrients and latitude drove peak intensity of greenness, a surrogate of plant biomass. GEI derived from time-lapse cameras was strongly associated with NDVI, serving as an inexpensive near-surface remote sensing platform to support and complement satellite observations. In this section, we discuss the characteristics of arctic wetland plants phenology, and the effects of climate and nutrients on greening. In addition, we comment on the relationships between camera-derived Green Excess Index (GEI), biomass and plot-level NDVI, as well as the technical limitations of using the GEI.

4.1. Climate and nutrient effects

Lengthening of growing season and a warming climate are factors known to influence plant species distribution (Grabherr et al., 1994; Walther et al., 2002). Our study suggests that increases in thawing degree-days from a warming climate are likely to promote the success

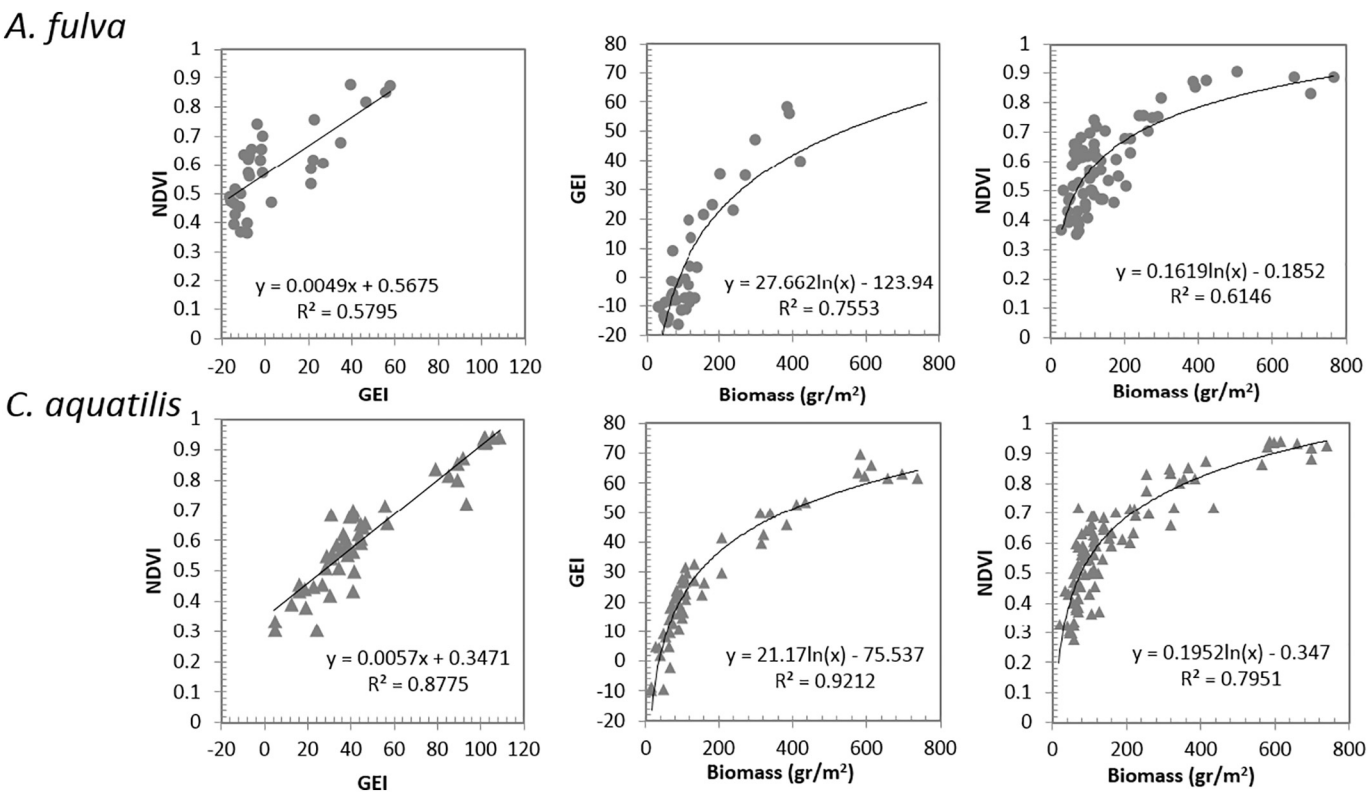

Fig. 3. Relationships between GEI (− 30° view angle from horizon) and NDVI (nadir view) and aboveground dry biomass for *Arctophila fulva* (top,circles) and *Carex aquatilis* (bottom, triangles). Data for NDVI and GEI are included for supplementary sites without phenocams.

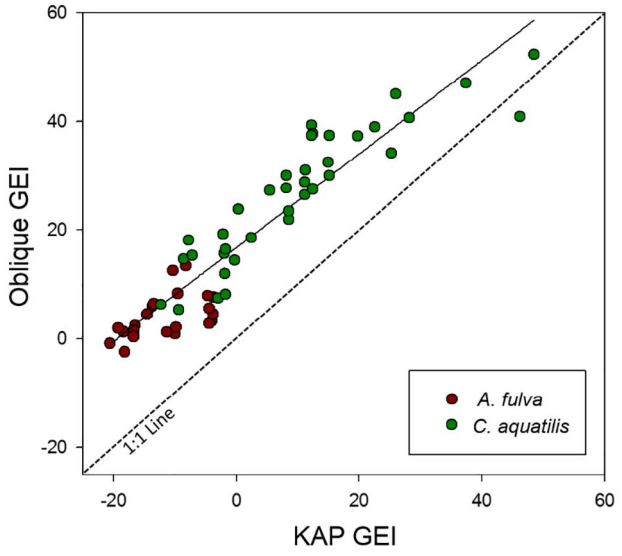

Fig. 4. Comparison between oblique angle GEI from phenocams and nadir angle Kite Aerial photography GEI of the phenocam footprint for sites IBP-J (*A. fulva* and *C. aquatilis*) and IBP-C (*C. aquatilis*) for the Jun–Aug season of 2010–2012. Black line across points indicates the linear fit for both plants.

of aquatic vegetation in the Arctic coastal plain, and may help explain the recent increase in biomass and cover of these species over the past 40 years (Andresen et al., 2017). *Arctophila fulva*, in particular, largely lacks any competition for habitat due to its adaptation to deep water, allowing colonization of new, untouched habitat and access to greater sources of nutrient supplies. However, short-term responses such as less biomass with earlier greening date found in this study for *A. fulva* contradict the long-term trends in increased biomass in the region (Andresen et al., 2017). In line with our findings, Gamon et al. (2013) found decreased vegetation growth following earlier snowmelt in the Utqiaġvik area wet sedge tundra. Perhaps vegetation productivity is being co-limited by nutrients and temperature, where the long-term increase in biomass for these species found by Andresen et al. (2017) is due to both increases in growing season length and release of nutrients from permafrost thaw (Reyes and Lougheed, 2015). Permafrost has been thawing in the study area (Shiklomanov et al., 2010), with thaw depth of ponds in Utqiaġvik having increased by about 11 cm over the past 60 years (Andresen and Lougheed, 2015). The total number of thawing degree-days has also increased by 13 days over the past 40 years (Andresen et al., 2017), which has likely enhanced permafrost thaw contributing to the observed increased in pond nutrients over recent decades (Lougheed et al., 2011).

This study shows that temperature and nutrients are factors controlling plant phenology in arctic aquatic systems and is in line with observations from other tundra plant communities (Borner et al., 2008; Oberbauer et al., 2013; Zeng et al., 2013). Greater greenness observed in enriched areas and lower latitude compared to reference sites further supports that both temperature and nutrients play a key role in enhancing productivity of these aquatic species. However, the latitude effect on timing of greening was not fully clear given the limited number of sites (n = 2) and years sampled (n = 1) for Atqasuk, which limited statistical analysis for greening dates. Further camera observations between Utqiaġvik and Atqasuk could help understand latitudinal differences. Enriched sites showed the highest greening followed by lower latitude sites, coincident with manipulation studies in wet sedges (Shaver et al., 1998; Boelman et al., 2003) that found the greatest change in fertilized treatments with little or null responses to warming treatments. In addition, we found that nutrient enriched sites exhibited extended peak greening in *C. aquatilis*, senescing later than reference sites (Fig. 5). No differences were observed for senescing in *A. fulva*. Our results support previous observations that tundra graminoids are strongly nutrient limited (Shaver et al., 1998). This is also supported by the higher aboveground biomass found in nutrient enriched sites

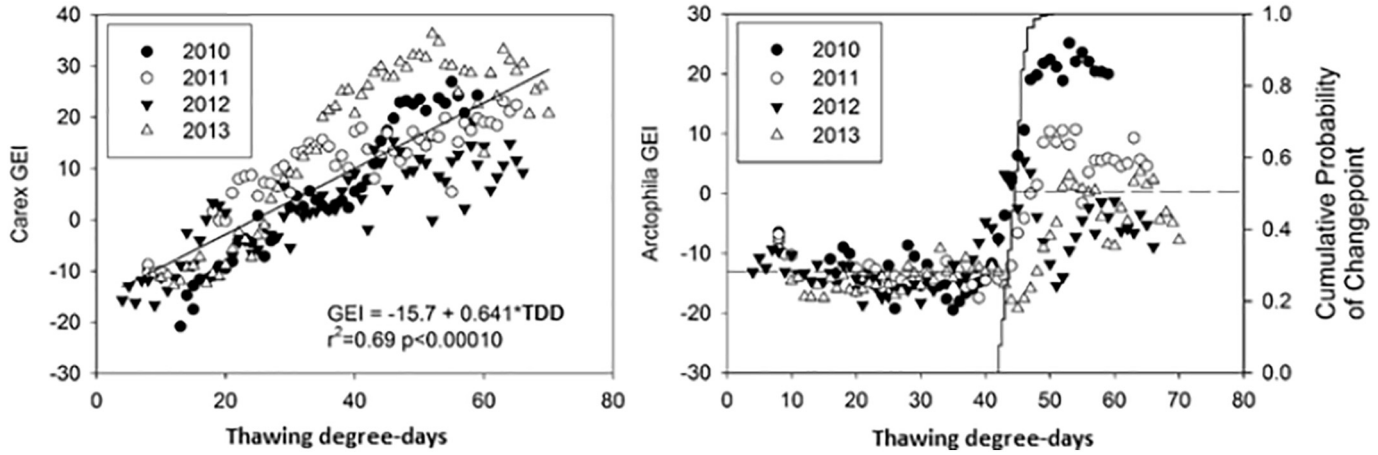

Fig. 5. Effects of the Thawing Degree-Days (TDD, days above 0 °C) on daily average GEI observations of reference sites sampled over multiple years (Pond-C, Pond-J and Pond-10) for *Carex aquatilis* (left; simple linear regression) and *Arctophila fulva* (right; regression tree). Vertical solid lines represent the threshold points of greening, as determined by regression tree, while dashed horizontal lines are the means for each partition.

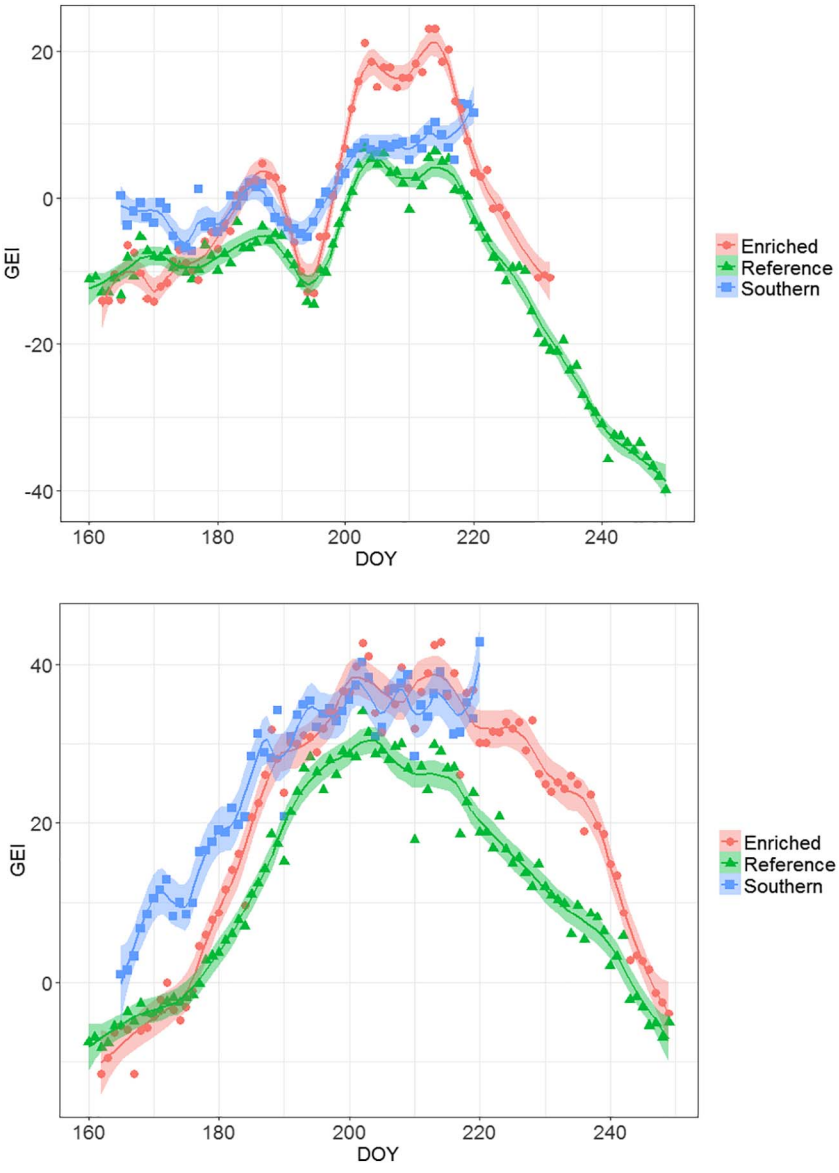

Fig. 6. Seasonal variability of average GEI among site types for *Arctophila fulva* (top) and *Carex aquatilis* (bottom)in 2013. In *A. fulva* GEI, Reference < South & Enriched ($p < 0.0001$). For *C. aquatilis* GEI, South > Enriched > Reference ($p < 0.0001$). Lines represent moving average of 2 days and shaded areas are 95% confidence intervals.

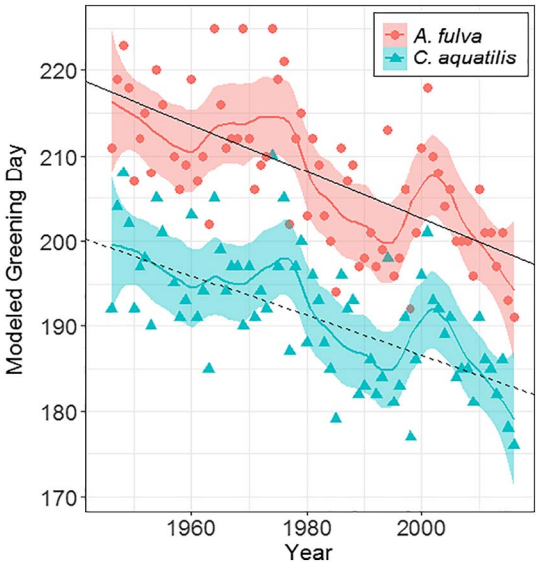

Fig. 7. Modeled greening date for *A. fulva* (circles) and *C. aquatilis* (triangles) using air temperature records from Barrow airport (http://climate.gi.alaska.edu/). Shaded area represents the 95% CI of the 5-year moving average line. (For interpretation of the references to color in this figure legend, the reader is referred to the web version of this article.)

compared to southern and reference sites, with similar soil and water nutrient levels (Andresen and Lougheed, unpublished data).

4.2. Arctophila fulva and Carex aquatilis phenology

The unique greening trends observed among different taxa (i.e. *C. aquatilis* and *A. fulva*) concurs with other studies that show taxa-specific greening timing (Richardson et al., 2009; Ide and Oguma, 2010). *C. aquatilis* demonstrated an early and gradual increase in greening after snowmelt attributed to the characteristic sequential leaf growth in *C. aquatilis* and other sedges (Tieszen, 1972; McRoy and Leue, 1973). On the other hand, *A. fulva* had a delayed but abrupt greening. Although *C. aquatilis* and *A. fulva* had different greening patterns, both species reached maximum greening during the same time period in late July. The overall lower GEI values observed for *A. fulva* compared to *C. aquatilis* are likely attributable to the red pigmentation and low chlorophyll concentrations characteristic of *A. fulva* (Tieszen, 1973).

The observed *A. fulva* greening date was on average 18 days after *C. aquatilis* suggesting a higher temperature optima compared to *C. aquatilis*. Cold events in mid-summer greatly affected plant greenness in *A. fulva* likely associated to physiological plant stress (Chapin, 1991) due to the reduction of photosynthesis as observed by the decrease in greenness, and likely, leaf nitrogen. We observed a decrease in GEI in 2011, 2012 and 2013 during peak season after cold fronts with the magnitude of change in GEI depending on the severity of the temperature decrease. Although greenness in *A. fulva* generally increased within ~5 days of a cold event, it never did recover completely to pre-event GEI greenness. *C. aquatilis* also showed decreases in greening after cold events during peak season but these dips were smaller than those observed for *A. fulva*. These observations also suggest that *A. fulva* may be more sensitive to cold temperatures as compared to *C. aquatilis*.

4.3. Biomass, green excess index and NDVI

Our study supports the use of color indices derived from time-lapse photography to assess plant biomass in aquatic emergent plants. We found that the GEI provided better resolution at higher plant biomass compared to NDVI. Although both NDVI and GEI asymptotically approached saturation with high biomass, GEI maintained a higher slope compared to the widely used NDVI (Gao et al., 2000; Viña et al., 2011); this comparison was most obvious for *A. fulva*. Given that regional biomass estimates in aquatic systems for *C. aquatilis* and *A. fulva* averaged 154.2 ± 19 and 144.7 ± 27 g/m^2 respectively (Andresen et al., 2017) and that these ranges are within the lower end of asymptotic curves, both GEI and NDVI are broadly suitable for these types of environments. However, differences among sites at the higher end of nutrient enrichment gradient may not be as easily distinguished with NDVI.

It is important to note that the comparison among NDVI and GEI is based on different viewing angles, where NDVI was measured perpendicular to the ground (nadir angle) while GEI was derived from an oblique angle of −30° from the horizon. We used NDVI at nadir to parallel satellite observations which are usually near-nadir and try to understand how oblique-view measurements from cameras associate with NDVI from a near-nadir satellite angle. Our results suggest that greenness was likely overestimated using an oblique GEI measurement as compared to NDVI, due to the exposure of more leaves overlapping within the footprint of the cameras. Aerial nadir view GEI measurements of the timelapse cameras footprint demonstrated relatively low values of GEI compared to the obliquely derived GEI estimates from time lapse cameras (Fig. 4). This suggests that GEI may not saturate compared to NDVI in high biomass conditions when measured from the same nadir angle.

The strong relationship between GEI and NDVI for both plant species concurs with previous studies (Westergaard-Nielsen et al., 2013) indicating the potential of GEI for assisting as a mid-level remote sensing platform to track seasonal trends in plant phenology (Kobayashi et al., 2016). However, in contrast to Westergaard-Nielsen et al. (2013), we tested the performance of GEI along a range of plant biomass. This ability to accurately assess biomass and NDVI with the high observation frequency of this method will aid satellite based observations that are usually limited by coverage and cloud cover in this Arctic region (Stow et al., 2004).

4.4. Limitations of GEI

Shifts in incident solar radiation, changing weather conditions and wind-driven movement of the plants were observed to contribute to changes in color channel brightness within short periods of time (e.g. minutes-hours). Our study minimized this variability by using constant white balance and daily GEI averages, greatly reducing day-to-day variability and allowing better sensitivity to seasonal changes in vegetation greenness (Richardson et al., 2009). Therefore, we attribute seasonal GEI changes to direct changes in greenness of plants as opposed as illumination effects sensed by the camera.

Changes in water level could be an important factor affecting GEI. These fluctuations may translate to the reduction or increment of the blue channel brightness sensed by the digital camera. Water level data (unpublished data) from four ponds across the Utqiaġvik area (IBP-J, IBP-B, ITEX-S, WL02) indicate a mean range in water level of 17 ± 7 cm for the ice-free season, which we considered minor with no major changes in the observed GEI values after rain events. This phenomenon should be taken into consideration for areas with major water level fluctuations and provide a corrective methodology for such events.

As any other multichannel index, GEI might be problematic for characterizing color in specific objects or conditions (e.g. water, snow, vegetation) since different matter may reflect wavelengths differently but in a way that can produce a similar GEI value. For example, the GEI value of open water conditions at the beginning of the season is dominated by the blue signal over the green, while vegetation senescence at the end of the season is dominated by the red channel over the green. These two very different conditions produce the same GEI value. Therefore, we advise careful evaluation of GEI depending on the season when the value was sensed.

It is important to note that commercial time-lapse cameras are not scientific-grade instruments and signal may differ among sensors. Individual cameras and camera models can have different non-linear responses to changes in brightness that may alter the RGB signal and thus, phenological signatures. For this study, we considered this issue to be non-critical given that images were acquired during solar noon and camera data was corrected for these brightness conditions using a gray standard calibration. However, future studies using multiple cameras and models at a large range of brightness levels should consider assessing the sensor responses to changes in brightness among cameras. Nonetheless, our methodology for inter-camera comparison may be an effective, semi-technical approach for relating multiple sensors. Gray standard targets have previously been used for assessing color balance in cameras (Richardson et al., 2009) and, for this study, proved to be a useful and inexpensive calibration tool improving standardization for inter-site greenness comparisons.

There is a lack of studies assessing how different cameras can be used to accurately determine differences among sites (Sonnentag et al., 2011, 2012). Therefore, this study provides a preliminary method for assessing future dynamics of vegetation phenology obtained from RGB color brightness levels with multiple sensors at different sites.

Different models have been suggested for estimation of greening and senescing dates depending mainly in the curve characteristics of seasonal greening trends. Curve fitting techniques such as quadratic functions have been employed for high Arctic regions given the short growing periods (Meltofte et al., 2008). Also, sigmoid curves have been widely employed in different environments (Richardson et al., 2009; Elmore et al., 2012; Granados et al., 2013) including the low Arctic (Westergaard-Nielsen et al., 2013). However, threshold-based estimation has proven to be more effective compared to curve-fitting models (Keenan et al., 2014). The threshold-based method used in our study proved to be an accurate system to identify GEI values that can be associated with key phenological changes for different species. Further comparison among curve-fitting and threshold approaches will provide a better insight into extracting phenological information from time series observations using time-lapse photography.

5. Conclusion

Our study shows that nutrients and climate are significant drivers of timing and intensity of plant phenology in Arctic wetlands. The continuing lengthening of the growing season combined with nutrients leached from permafrost thaw will likely enhance primary productivity in Arctic wetlands. This phenomenon will have significant implications in the carbon budget, particularly on the increased of methane emissions (Andresen et al., 2017).

The need for high-frequency monitoring of plant phenology in Arctic wetlands motivated this study to develop a novel system that employs time-lapse photography as a near-surface remote sensing method to track seasonal plant biomass and greening of aquatic emergent graminoids in the Arctic. This novel automated method proved to be a reliable and cost-effective alternative for continual monitoring of biomass and greening in aquatic plants, as well as assessing nutrient and climate effects in aquatic plant phenology. The integration of near-surface observations (i.e. time-lapse photography) with mid-level (i.e. unmanned aerial systems) and satellite-level remote sensing platforms promises to greatly advance understanding of arctic wetlands.

The future of arctic wetlands is uncertain given the projected increase in permafrost thaw, which will likely decrease surface water saturation (Avis et al., 2011). Therefore, it is imperative that we continue developing and advancing monitoring systems such as the one presented in this study to further understand these ecological-important ecosystems in the Arctic, with the ultimate goal to refine global coupled models and better predict future climatic scenarios.

Acknowledgements

This study was funded by the National Science Foundation (NSF) Graduate Research Fellowship Program to CGA (NSF-1110312) and research funding to VLL (ARC-0909502). Thanks to Giovani Ramirez for his assistance in the image processing, and to Frankie Reyes, Christina Hernandez, and Nickole Miller for their help in the field. UMIAQ, the Barrow Arctic Science Consortium (BASC) and the Ukpeagvik Inupiaq Corporation (UIC) provided logistical support and land access.

References

Ahrends, H., Etzold, S., Kutsch, W., et al., 2009. Tree phenology and carbon dioxide fluxes: use of digital photography for process-based interpretation at the ecosystem scale. Clim. Res. 39, 261–274.
Andresen, C.G., 2014. Monitoring and Understanding Decadal Scale Changes in Hydrology, Productivity and Carbon Balance in Arctic Tundra Ponds. University of Texas at El Paso (108 pp).
Andresen, C.G., Lougheed, V.L., 2015. Disappearing arctic tundra ponds: fine-scale analysis of surface hydrology in drained thaw lake basins over a 65 year period (1948–2013). J. Geophys. Res. 120, 1–14.
Andresen, C.G., Vargas, S.A., Lougheed, V.L., Tweedie, C.E., 2014. Kite-based aerial photography (KAP): a low cost, effective tool for wetland research. Wetl. Sci. Pract. 32, 15–19.
Andresen, C.G., Lara, M.J., Tweedie, C.T., Lougheed, V.L., 2017. Rising plant-mediated methane emissions from arctic wetlands. Glob. Chang. Biol. 23, 1128–1139.
Avis, C.A., Weaver, A.J., Meissner, K.J., 2011. Reduction in areal extent of high-latitude wetlands in response to permafrost thaw. Nat. Geosci. 4, 444–448.
Bhatt, U.S., Walker, D.A., Raynolds, M.K., et al., 2010. Circumpolar arctic tundra vegetation change is linked to sea ice decline. Earth Interact. 14, 1–20.
Boelman, N.T., Stieglitz, M., Rueth, H.M., Sommerkorn, M., Griffin, K.L., Shaver, G.R., J a, Gamon, 2003. Response of NDVI, biomass, and ecosystem gas exchange to long-term warming and fertilization in wet sedge tundra. Oecologia 135, 414–421.
Boelman, N.T., Stieglitz, M., Griffin, K.L., Shaver, G.R., 2005. Inter-annual variability of NDVI in response to long-term warming and fertilization in wet sedge and tussock tundra. Oecologia 143, 588–597.
Borner, A.P., Kielland, K., Walker, M.D., 2008. Effects of simulated climate change on plant phenology and nitrogen mineralization in alaskan arctic tundra. Arct. Antarct. Alp. Res. 40, 27–38.
Brown, T.B., Hultine, K.R., Steltzer, H., et al., 2016. Using phenocams to monitor our changing Earth: toward a global phenocam network. Front. Ecol. Environ. 14, 84–93.
Callaghan, T.V., Christensen, T.R., Jantze, E.J., 2011. Plant and vegetation dynamics on Disko Island, West Greenland: snapshots separated by over 40 years. Ambio 40, 624–637.
Chapin, F.S., 1991. Integrated responses of plants to stress. Bioscience 41, 29–36.
Cowardin, L.M., Carter, V., Golet, F.C., LaRoe, E.T., 1979. Classification of Wetlands and Deepwater Habitats of the United States. FGDC-STD-004-2013. Second Edition. 79.
Stow, D.A., Hope, A., McGuire, D., et al., 2004. Remote sensing of vegetation and land-cover change in Arctic Tundra Ecosystems. Remote Sens. Environ. 89, 281–308.
Dobson, J.L., 1989. Autecology of Aquatic and Terrestrial Growth Forms of *Arctophila fulva*, an Arctic Tundra Grass of Northern Alaska. University of Idaho, Moscow, ID, US.
Elmendorf, S.C., Henry, G.H.R., Hollister, R.D., et al., 2012. Global assessment of experimental climate warming on tundra vegetation: heterogeneity over space and time. Ecol. Lett. 15, 164–175.
Elmore, A.J., Guinn, S.M., Minsley, B.J., Richardson, A.D., 2012. Landscape controls on the timing of spring, autumn, and growing season length in mid-Atlantic forests. Glob. Chang. Biol. 18, 656–674.
Epstein, H.E., Raynolds, M.K., Walker, D.A., Bhatt, U.S., Tucker, C.J., Pinzon, J.E., 2012. Dynamics of aboveground phytomass of the circumpolar Arctic tundra during the past three decades. Environ. Res. Lett. 7, 15506.
Gamon, J.A., Huemmrich, K.F., Stone, R.S., Tweedie, C.E., 2013. Spatial and temporal variation in primary productivity (NDVI) of coastal Alaskan tundra: decreased vegetation growth following earlier snowmelt. Remote Sens. Environ. 129, 144–153.
Gao, X., Huete, A., Ni, W., Miura, T., 2000. Optical–biophysical relationships of vegetation spectra without background contamination. Remote Sens. Environ. 74, 609–620.
Grabherr, G., Gottfried, M., Pauli, H., 1994. Climate effects on mountain plants. Nature 369, 448.
Granados, J.A., Graham, E.A., Bonnet, P., Yuen, E.M., Hamilton, M., 2013. EcoIP: an open source image analysis toolkit to identify different stages of plant phenology for multiple species with pan–tilt–zoom cameras. Eco. Inform. 15, 58–65.
Healey, N.C., Oberbauer, S.F., Ahrends, H.E., et al., 2014. A mobile instrumented sensor platform for long-term terrestrial ecosystem analysis: an example application in an arctic tundra ecosystem. J. Environ. Inform. 24, 1–10.
Hinkel, K., Eisner, W., JG, B., Nelson, F.E., Peterson, K.M., Xiaoyan, D., 2003. Spatial extent, age, and carbon stocks in drained thaw lake basins on the Barrow Peninsula, Alaska. Arct. Antarct. Alp. Res. 35, 291–300.
Hinzman, L.D., Deal, C.J., McGuire a, D., Mernild, S.H., Polyakov, I.V., Walsh, J.E., 2013. Trajectory of the Arctic as an integrated system. Ecol. Appl. 23, 1837–1868.
Ide, R., Oguma, H., 2010. Use of digital cameras for phenological observations. Eco. Inform. 5, 339–347.

Jia, G.J., 2003. Greening of arctic Alaska, 1981–2001. Geophys. Res. Lett. 30, 2067.
Keenan, T., Darby, B., Felts, E., 2014. Tracking forest phenology and seasonal physiology using digital repeat photography: a critical assessment. Ecol. Appl. 24, 1478–1489.
Kobayashi, H., Yunus, A.P., Nagai, S., et al., 2016. Latitudinal gradient of spruce forest understory and tundra phenology in Alaska as observed from satellite and ground-based data. Remote Sens. Environ. 177, 160–170.
Kurc, S.A., Benton, L.M., 2010. Digital image-derived greenness links deep soil moisture to carbon uptake in a creosotebush-dominated shrubland. J. Arid Environ. 74, 585–594.
Lehner, B., Döll, P., 2004. Development and validation of a global database of lakes, reservoirs and wetlands. J. Hydrol. 296, 1–22.
Lougheed, V.L., Parker, C.A., Stevenson, R.J., 2007. Using non-linear responses of multiple taxonomic groups to establish criteria protective of wetland biological condition. Wetlands 27, 96–106.
Lougheed, V.L., Butler, M.G., McEwen, D.C., Hobbie, J.E., 2011. Changes in Tundra pond limnology: re-sampling Alaskan ponds after 40 years. Ambio 40, 589–599.
Lougheed, V.L., Hernandez, C., Andresen, C.G., Miller, N.A., Alexander, V., Prentki, R., 2015. Contrasting responses of phytoplankton and benthic algae to recent nutrient enrichment in Arctic tundra ponds. Freshw. Biol. 60, 2169–2186.
McRoy, C.P., Leue, T.S., 1973. Productivity of emergent vascular aquatic plants in Tundra ponds in 1971 and 1972. In: Data Report 73–8. 15 pp. U.S. Tundra Biome (15 pp).
Meltofte, H., Christensen, T.R., Elberling, B., Forchammer, M., Rasch, M., 2008. High-Arctic Ecosystem Dynamics in a Changing Climate. Academic Press (596 pp).
Melton, J.R., Wania, R., Hodson, E.L., et al., 2013. Present state of global wetland extent and wetland methane modelling: conclusions from a model inter-comparison project (WETCHIMP). Biogeosciences 10, 753–788.
Migliavacca, M., Galvagno, M., Cremonese, E., et al., 2011. Using digital repeat photography and eddy covariance data to model grassland phenology and photosynthetic CO_2 uptake. Agric. For. Meteorol. 151, 1325–1337.
Nagai, S., Ichie, T., Yoneyama, A., et al., 2016. Usability of time-lapse digital camera images to detect characteristics of tree phenology in a tropical rainforest. Eco. Inform. 32, 91–106.
Nijland, W., Bolton, D.K., Coops, N.C., Stenhouse, G., 2016. Imaging phenology; scaling from camera plots to landscapes. Remote Sens. Environ. 177, 13–20.
Oberbauer, S.F., Elmendorf, S.C., Troxler, T.G., et al., 2013. Phenological response of tundra plants to background climate variation tested using the International Tundra Experiment. Philos. Trans. R. Soc. Lond. Ser. B Biol. Sci. 368, 20120481.
Prowse, T.D., Wrona, F.J., Reist, J.D., Gibson, J.J., Hobbie, J.E., Lévesque, L.M.J., Vincent, W.F., 2006. Climate change effects on hydroecology of arctic freshwater ecosystems. Ambio 35, 347–358.
Reyes, F.R., Lougheed, V.L., 2015. Rapid nutrient release from permafrost in Arctic aquatic ecosystems. Arct. Antarct. Alp. Res. 47, 35–48.
Richardson, A.D., Braswell, B.H., Hollinger, D.Y., Jenkins, J.P., Ollinger, S.V., 2009. Near-surface remote sensing of spatial and temporal variation in canopy phenology. Ecol. Appl. 19, 1417–1428.
Saitoh, T.M., Nagai, S., Saigusa, N., Kobayashi, H., Suzuki, R., Nasahara, K.N., Muraoka, H., 2012. Assessing the use of camera-based indices for characterizing canopy phenology in relation to gross primary production in a deciduous broad-leaved and an evergreen coniferous forest in Japan. Eco. Inform. 11, 45–54.
Shaver, G.R., Johnson, L.C., Cades, D.H., et al., 1998. Biomass and flux in wet sedge Tundras: responses to nutrients, temperature, and light. Ecol. Monogr. 68, 75–97.
Shiklomanov, N.I., Streletskiy, D.A., Nelson, F.E., et al., 2010. Decadal variations of active-layer thickness in moisture-controlled landscapes, Barrow, Alaska. J. Geophys. Res. 115, G00I04.
Smol, J.P., Douglas, M.S.V., 2007. Crossing the final ecological threshold in high Arctic ponds. Proc. Natl. Acad. Sci. U. S. A. 104, 12395–12397.
Sonnentag, O., Detto, M., Vargas, R., Ryu, Y., Runkle, B.R.K., Kelly, M., Baldocchi, D.D., 2011. Tracking the structural and functional development of a perennial pepperweed (*Lepidium latifolium* L.) infestation using a multi-year archive of webcam imagery and eddy covariance measurements. Agric. For. Meteorol. 151, 916–926.
Sonnentag, O., Hufkens, K., Teshera-Sterne, C., et al., 2012. Digital repeat photography for phenological research in forest ecosystems. Agric. For. Meteorol. 152, 159–177.
Soudani, K., Hmimina, G., Delpierre, N., et al., 2012. Ground-based network of NDVI measurements for tracking temporal dynamics of canopy structure and vegetation phenology in different biomes. Remote Sens. Environ. 123, 234–245.
Sturm, M., Racine, C., Tape, K., Cronin, T.W., Caldwell, R.L., Marshall, J., 2001. Increasing shrub abundance in the Arctic. Nature 411, 2001–2002.
Tape, K.D., Sturm, M., Racine, C.H., 2006. The evidence for shrub expansion in Northern Alaska and the Pan-Arctic. Glob. Chang. Biol. 12, 686–702.
Tieszen, L.L., 1972. The seasonal course of aboveground production and chlorophyll distribution in a wet Arctic tundra at Barrow, Alaska. Arct. Alp. Res. 4, 307–324.
Tieszen, L., 1973. Photosynthesis and respiration in arctic tundra grasses: field light intensity and temperature responses. Arct. Alp. Res. 5, 239–251.
Villarreal, S., Hollister, R.D., Johnson, D.R., Lara, M.J., Webber, P.J., Tweedie, C.E., 2012. Tundra vegetation change near Barrow, Alaska (1972–2010). Environ. Res. Lett. 7, 15508.
Viña, A., Gitelson, A.A., Nguy-Robertson, A.L., Peng, Y., 2011. Comparison of different vegetation indices for the remote assessment of green leaf area index of crops. Remote Sens. Environ. 115, 3468–3478.
Walker, M.D., Wahren, C.H., Hollister, R.D., et al., 2006. Plant community responses to experimental warming across the tundra biome. Proc. Natl. Acad. Sci. U. S. A. 103, 1342–1346.
Walker, D.A., Epstein, H.E., Raynolds, M.K., et al., 2012. Environment, vegetation and greenness (NDVI) along the North America and Eurasia Arctic transects. Environ. Res. Lett. 7, 15504.
Walther, G., Post, E., Convey, P., Menzel, A., 2002. Ecological responses to recent climate change. Nature 389–395.
Westergaard-Nielsen, A., Lund, M., Hansen, B.U., Tamstorf, M.P., 2013. Camera derived vegetation greenness index as proxy for gross primary production in a low Arctic wetland area. ISPRS J. Photogramm. Remote Sens. 86, 89–99.
Woo, M., Young, K.L., 2006. High Arctic wetlands: their occurrence, hydrological characteristics and sustainability. J. Hydrol. 320, 432–450.
Zeng, H., Jia, G., 2013. Impacts of snow cover on vegetation phenology in the arctic from satellite data. Adv. Atmos. Sci. 30, 1421–1432.
Zeng, H., Jia, G., Forbes, B., 2013. Shifts in Arctic phenology in response to climate and anthropogenic factors as detected from multiple satellite time series. Environ. Res. Lett. 8, 35036.